

UCSF

UC San Francisco Previously Published Works

Title

MRI Atlas-Based Measurement of Spinal Cord Injury Predicts Outcome in Acute Flaccid Myelitis

Permalink

<https://escholarship.org/uc/item/5vj3f1gf>

Journal

American Journal of Neuroradiology, 38(2)

ISSN

0195-6108

Authors

McCoy, DB

Talbott, JF

Wilson, Michael

et al.

Publication Date

2017-02-01

DOI

10.3174/ajnr.a5044

Peer reviewed



MRI atlas-based measurement of spinal cord injury predicts outcome in acute flaccid myelitis

Journal:	<i>American Journal of Neuroradiology</i>
Manuscript ID	Draft
Manuscript Type:	Original Research
Classifications:	Spine: infection < Spine, Statistics: outcomes < Statistics, CS: image postprocessing < Computer Science (CS)

SCHOLARONE™
Manuscripts

Review



1001 Potrero Avenue
San Francisco, CA 94110

Phone (415) 206-8000
Fax (415) 206-6922

ZuckerbergSanFranciscoGeneral.org

JARED NARVID, M.D.
ASSISTANT PROFESSOR IN RADIOLOGY
DEPARTMENT OF RADIOLOGY & BIOMEDICAL IMAGING
ZUCKERBERG SAN FRANCISCO GENERAL HOSPITAL

PHONE: (415) 206-5880
FAX: (415) 206-4004
SAN FRANCISCO, CA 94110
E-MAIL: JARED.NARVID@UCSF.EDU

April 1, 2016

Jeffrey S. Ross, MD, Editor-in-chief, *American Journal of Neuroradiology*
Department of Radiology
St. Joseph Hospital and Medical Center
350 W Thomas Road
Phoenix, AZ 85013

Dear Dr. Ross:

We respectfully submit a manuscript entitled, “**MRI atlas-based measurement of spinal cord injury predicts outcome in acute flaccid myelitis**” for consideration to *AJNR*. We have not submitted this manuscript to any other journal and we believe this manuscript significantly advances the literature related to both quantitative spinal cord imaging as well as infectious myelitis.

All authors contributed to the research and writing of this manuscript and agree with the submission. The research was approved by the hospital’s committee on Human Subjects research. Financial disclosures include (1) JFT: member of StemCells, Inc. data monitoring committee.

We believe that this submission will alert the readership of *AJNR* to the potential value in utilizing tools such as the Spinal Cord toolbox and perhaps more so, the vital role radiology plays in diagnosis and prognostication for patients with acute flaccid paralysis. We appreciate your kind consideration of our manuscript.

Sincerely,

Jared Narvid, MD



ScholarOne Support: (434) 964-4100

MRI atlas-based measurement of spinal cord injury predicts outcome in acute flaccid myelitis

David B. McCoy¹, Jason F. Talbott^{1,2}, Michael Wilson⁵, Mark Mamlouk¹, Julien Cohen-Adad^{3,4}, Mark Wilson¹, Jared Narvid¹

¹Department of Radiology and Biomedical Imaging, University of California, San Francisco Zuckerberg San Francisco General Hospital, San Francisco, CA.

²Brain and Spinal Injury Center, San Francisco General Hospital, San Francisco, CA

³Institute of Biomedical Engineering, Ecole Polytechnique, Montreal, QC, Canada

⁴Functional Neuroimaging Unit, CRIUGM, University of Montreal, Montreal, QC, Canada

⁵Department of Neurology, University of California, San Francisco

Please address correspondence and reprint requests to

Jared A. Narvid, M.D.
Assistant Professor of Radiology and Biomedical Imaging
University of California at San Francisco
Zuckerberg San Francisco General
Hospital and Trauma Center
jared.narvid@ucsf.edu
415.206.5880
1001 Potrero Ave Room 1x57, SFGH Box 1325
San Francisco, CA 94110

ABSTRACT

Background/objective: Recent advances in spinal cord (SC) imaging analysis have led to the development of a robust anatomical template and atlas incorporated into an open-source platform referred to as the Spinal Cord Toolbox (SCT). Utilizing the SCT, we sought to correlate measures of gray matter (%GM), white matter (%WM), and cross-sectional area (%CSA) pathology on T2-MRI with motor disability in patients with acute flaccid myelitis (AFM).

Methods: SC imaging for nine patients with AFM were analyzed using the SCT. A semi-automated pipeline utilizing the SCT measured lesion involvement in GM, WM and total SC CSA. %GM, %WM and %CSA affected by T2 hyperintensity were calculated across three regions of interest i.) center axial slice of lesion, ii.) full lesion segment, and iii.) full cord atlas volume. Spearman rank order correlation was calculated to compare MR metrics with clinical measures of disability.

Results: %GM metrics at the center axial slice significantly correlated with measures of motor impairment upon admission ($r_s(9)=-.78$ $p=0.014$) and at 3 month follow-up ($r_s(9)=-0.66$ $p = .05$). Further, %GM extracted across the full lesion segment significantly correlated with initial motor impairment ($r_s[9] = -.74$ $p=0.024$). No significant correlation was found for %WM or %CSA with clinical disability.

Conclusions: Atlas-based measures of %GM T2-signal abnormality measured on a single axial MRI slice and across the full lesion segment correlate with motor impairment and outcome in patients with AFM. This is the first atlas-based study to correlate clinical outcomes with segmented measures of T2-signal abnormality in the SC.

INTRODUCTION

After the eradication of wild poliovirus, the clinical syndrome of spinal motor neuron injury called AFM nearly disappeared from North America. The re-emergence of this syndrome has coincided with appearance of West Nile Virus in Europe and North America, enterovirus (EV) A71 in Southeast Asia, and EV D68 in North America^{1,2}. In fact, at the same time as EV D68 caused widespread outbreaks of respiratory illness in the US in 2014, the number of AFM cases spiked³. The Centers for Disease Control and Prevention noted this association describing the incidence of AFM, a subset of acute flaccid paralysis cases with evidence of spinal cord injury.

More recently, longitudinally extensive spinal cord lesions predominantly affecting the central gray matter have been described in children with AFM during the 2014 EV outbreak⁵. The prognosis in such cases is variable with few predictors of recovery aside from the severity of initial paralysis. However, in a variety of spinal cord pathologies, defining the pattern and extent of signal abnormality on MRI can aid in diagnosis and prognosis⁶.

The recent development of a standard spinal cord template⁷ – as part of the Spinal Cord Toolbox (SCT)⁸ – that includes probabilistic maps of gray matter and white matter⁹ now makes it possible to quantify the severity of spinal cord injury¹⁰⁻¹². We aimed to measure the proportion of gray matter and white matter damaged in patients with AFM occurring in association with the EV-D68 outbreak. We hypothesize that the degree of gray and white matter injury in these patients would both correlate with severity of initial symptoms and symptoms at follow-up, after hospitalization. Although several studies have investigated the association between GM/WM pathology on MRI and disease severity¹³⁻¹⁸; to date, this is first study using this analysis method to register spinal cords with abnormal signal to an unbiased average anatomical template, quantify %GM, %WM, and %CSA occupied by lesion in the probabilistic template, and correlate data with clinical outcomes.

Methods

Case Definition

All patients (9 total) admitted to the Benioff Children's Hospital at UCSF with acute flaccid myelitis (AFM) were included in the study. Dates of hospital admission ranged from February 12, 2012 to February 2, 2015. All study patients met the clinical case definition of AFM as described by the Centers of Disease Control. Cases were defined as acute limb weakness with MRI spinal cord abnormality. Other infectious causes of AFM were excluded including Gullain-Barré syndrome, West Nile virus, Poliovirus, stroke, transverse myelitis,

myasthenia gravis and botulism. Nasopharyngeal swab, oropharyngeal swab, serum, stool, or cerebrospinal fluid samples were tested for enterovirus RNA using polymerase chain reaction (PCR) for all patients. Enterovirus PCR was conducted at ViraCor for three patients, California Department of Public Health – Neurologic Testing and Surveillance Viral & Rickettsial Disease Laboratory for two patients, Kaiser Permanente Medical Group for two patients, Lucile Packard Children’s Hospital for one patient and Stanford University Hospitals for one patient.

During initial hospitalization, all patients underwent complete neurologic testing. Strength testing was formalized using the Composite Medical Research Council (MRC) Scale for Muscle Strength Scores using 3 proximal muscles and 2 distal muscles in the affected limb for a score ranging 0-25. At follow-up MRC strength testing was repeated and recorded. Improvement in strength was recorded as the numerical difference in MRC score.

Local institutional review board approval was obtained through the University of California San Francisco Committee on Human Research for retrospective review and analysis of patient clinical information and magnetic resonance images.

MRI Acquisition Parameters

All MRI studies were performed on a 1.5 Tesla GE Genesis HDxt Signa scanner with software version 15 (GE Healthcare, Milwaukee, WI). Axial and Sagittal T2 fast spin echo (FSE) imaging was performed with the following parameters (presented as mean values \pm standard deviation from all 9 exams) TR=3398.78ms \pm 1430.99ms, TE= 99.04ms \pm 12.93ms, slice thickness=3.33mm, echo train length (ETL)=18.56 \pm 3.28. Average native plane resolution after interpolation of images (2D \rightarrow 3D), X=0.40, Y=0.40, Z=4.17. Additional sequences performed as part of our routine Spine and Brain MRI protocol were not evaluated for purposes of this study.

Image Processing

T2 weighted images for nine AFM patients were analyzed with the Spinal Cord Toolbox. The FMRIB Software Library v5.0¹⁹ (FSL) viewer module was used to manually mark the seed points for analysis. These locations flag the beginning and end regions for the propagation deformation model to segment the spinal cord²⁰. During automatic segmentation, detection of the spinal cord is done in the axial plane using the Hough transform. This is followed by propagation of an elliptical triangular tubular mesh built inside the spinal cord. The tubular mesh is then deformed towards the edges of the SC²⁰. Results of segmentation accuracy were unsatisfactory due to the large signal hyperintensity in this cluster of patients. Because of this, initial segmentation of each spinal cord

was done manually by creating images of spinal cord voxel locations using FSL and using two centerline points to mark the beginning and end axial slices for registration. Registration to the template took roughly 540 seconds per patient. The SCT automatic pipeline to register, warp, and extract WM and GM metrics for each SC consisted of (Figure 1):

1. A 3D labels file was created based on the coordinates of the first (C2/C3) and last (to T6) vertebral level landmarks to be analyzed using the spinal cord labeling utility.
2. A 3D mask file was created manually in FSL to identify voxels within the spinal cord. SC masks were confirmed by two radiologists as identifying only areas within the SC.
3. A combination of affine and non-linear registrations were done of the T2-weighted image to the corresponding MNI-Poly-AMU template. The MNI-Poly-AMU template is an image of the SC averaged across multiple individuals and is used as a reference point for registration of patient SCs and atlas-based MR signal quantification⁷. Registration was done in four steps. In step 1, a non-linear transformation is estimated to straighten the spinal cord (in order to match the MNI-Poly-AMU straight template). In step 2, an affine transformation is found based on the input labels to match the vertebral levels between the subject and the template. In step 3, a 2D slice-wise registration is done to bring the subject closer to the template, while ensuring robustness towards pathology by using the cord segmentation instead of the image, using mean squares metric and smoothing factor of 2. In step 4, local registration adjustment were made using B-Spline SyN algorithm with mean squares metric, gradient step of 0.5, smoothing factor of 0, with 5 iterations. The outputs were a T2-weighted image warped to the template and a template warped to the T2-weighted image, along with a pair of forward and reverse deformation fields.
4. The reverse deformation field (template → subject) were then applied to the WM and GM atlases, projecting them in the subject space. These warping fields are used to register multi-parametric data to a common space for quantification of image-derived metrics.
5. Raw images were thresholded to provide binary ROI of lesion area for analysis with the WM/GM and SC probabilistic atlases. Thresholding of images was performed in FSL with manual percentile adjustment to segment the lesions from surrounding normal appearing SC. Thresholded T2 images were confirmed by two neuroradiologists who were blinded to clinical data, segmenting only areas affected by lesions. Metrics were extracted using spinal cord toolbox extract metric function of the spinal cord toolbox. The percentage of lesion within GM/WM and SC probabilistic atlas voxel space was extracted as a weighted average restrained to values > 0.5 using the thresholded MR images.
6. Weighted average metrics and the corresponding standard deviations were extracted from the lesion axial center, lesion segment, and full cord

atlas volume. The use of a binary image of lesion area in this analysis is used to summate the voxel-wise probabilities occupied by the lesion per axial slice.

7. Spearman's rho (r_s), p-values, linear regression slopes and intercepts were calculated using numpy and matplotlib in python. Regression plots and bar charts were also plotted using matplotlib.

Atlas-based Spinal Cord Injury Assessment

Probabilistic maps were created for all nine patients containing all cervical levels and extending to thoracic level 6. For analysis at the lesion center, two neuroradiologists (JN and JFT) reviewed each SC image and identified the axial slice showing the most significant T2 hyperintensity; so-called lesion center. In one patient, the lesion center showing the most extensive hyperintensity could not be analyzed due to it being below T6. In this case (patient 1) the next most severely affected region was analyzed. For analysis of the full lesion segment, sagittal T2 images were used to identify the starting and ending axial slice where the lesion was involved (Figure 1). In the full cord atlas volume analysis, the entire length of thresholded spinal cord within the probabilistic atlases was used. Weighted averages of GM, WM and SC affected by lesion at the center axial slice, full lesion segment and full cord atlas volume for each patient are described in Table 2. A Spearman's Rank-Order Correlation was used to determine if metrics from each lesion analysis significantly correlated with MRC strength scores or clinical outcome scores.

Statistical Analysis

Composite Medical Research Council Scale (MRC) for Muscle Strength Scores, clinical outcomes scores and weighted averages of the binary thresholded image in probabilistic GM and WM voxel space were used in a Spearman's Rank-Order Correlation. P-values comparing patients testing EV positive and EV negative were calculated using Mann-Whitney U test. Furthermore, Mann-Whitney U tests for medians were used to determine if GM and WM weighted average metrics were significantly different between outcome and MRC groups. Independent-Samples Kruskal-Wallis Test on GM metrics was used to compare groups.

RESULTS

Clinical Findings

Patients were of age 2 to 27 at time of study, with a majority of patients being under 10 years of age (6 male, 3 female). The patient demographics, discharge diagnosis, MRC composite score and clinical outcome rating are detailed in Table 1. Among the nine patients, four patients presented with bilateral lower extremity flaccidity, three patients presented with left upper

extremity flaccidity and two patients with right upper extremity flaccidity. Additional presenting symptoms included fever (8 cases), URI (4 cases), bodily pain/pruritus/allodynia/abnormal sensation (5 cases), nausea/PO intolerance/emesis (3 cases), urinary retention (2 cases), ataxia (1 case). Enteroviral polymerase chain reaction of the CSF was negative in all patients. Nasopharyngeal swabs tested positive for EV RNA for two patients and serum samples for one patient tested positive for EV. One nasopharyngeal swab sample was positively subtyped as EV-D68. Mean clinical follow-up time was 396.33 days (Interquartile range, 100.00).

MRI Findings

All patients had spinal cord lesions involving the central cord gray matter and some degree of surrounding white matter. Lesions consisted of well-defined T2 hyperintensity primarily involving the anterior horn cells for four patients (1,2,4,9) and ill-defined lesions affecting the entire central spinal cord gray matter for five patients (3,5,6,7,8) (Figure 2). In one case, ill-defined T2 hyperintensity extended the entire length of the spinal cord. Patients with most longitudinally extensive hyperintensity throughout both cervical and thoracic areas had bilateral flaccid lower extremities. On MR T2 images, brain lesions were identified in two patients. One patient showed hyperintensity in the right frontal lobe. The second patient showed brainstem and thalamic edema.

Spinal Cord Analysis

MR spinal cord injury metrics were calculated for each patient (Table 2). Measuring at the center of the lesion (lesion center slice), clinical outcome significantly worsened as %GM increased ($r_s[9] = -.66, p = .05$) (Figure 3). Similarly the %GM injured showed significant correlation with weakness at initial examination for both lesion center measurement ($r_s[9] = -.78, p = .014$) and full lesion segment volume measurements ($r_s[9] = -.74, p = .024$). There was no significant association between %WM injured and clinical outcome or MRC strength scores at lesion center or full lesion segment volume. In full cord atlas volume analysis, neither GM nor WM significantly correlated with either improvement or initial weakness. No significant correlation was found between %CSA at lesion center and clinical outcome ($r_s[9] = 0.03, p = 0.95$) or initial MRC score ($r_s[9] = -.46, p = 0.213$). Furthermore, weighted averages extracted for %CSA at lesion segment did not significantly correlate with clinical outcome ($r_s[9] = -0.05, p = 0.89$) or initial MRC score ($r_s[9] = -.25, p = 0.52$). No significant differences were found between the EV positive versus negative groups or among clinical outcome groups in the degree of initial weakness (strength score), extent of GM or WM injury in either lesion center or full lesion segment volume.

DISCUSSION

In the present study, we have utilized a semi-automated analysis pipeline to quantify T2 signal abnormality in the spinal cord of patients diagnosed with AFM. More specifically, T2-weighted MRI sequences from 9 patients with AFM were successfully registered to the recently developed MNI-Poly-AMU spinal cord template. Using the associated SC Toolbox, measures of %GM, %WM and %CSA pathologic T2 signal hyperintensity were derived after thresholded T2 images segmented relative to pathologic signal were compared with probabilistic GM, WM, and SC maps from the SC toolbox. The primary aim of this study was to determine the feasibility and prognostic validity of implementing an atlas-based approach for MRI analysis in a population of AFM patients. To this end, the positive correlations observed between SCT-derived MRI metrics of GM pathology and clinical outcome validate this approach. While atlas-based analysis techniques have been applied to a variety of brain pathologies²¹⁻²³, this is the first study to implement an atlas-based approach for study of WM and GM specific pathology in the spinal cord.

Patients with AFM occurring in association with a recent EV D-68 outbreak were studied because this type of myelopathy distinctively targets central gray matter, primarily the anterior horn cells²¹. Accordingly, an atlas that allows specific evaluation of gray matter signal abnormality would improve our ability to assess degree of injury and prognosis. In precisely this way, %GM signal abnormality on a single axial slice at the injury center most strongly correlated with neurologic impairment, while statistically insignificant correlations were seen with measures of %WM and %CSA injury. This is despite the presence of T2 signal abnormality involving white matter to a varying degree in all patients. These findings are consistent with the presumed underlying pathophysiology of disease in this cohort of patients, wherein anterior horn cells of spinal cord gray matter are particularly vulnerable to enteroviral toxicity and manifestations of their injury would be expected to best predict outcome²⁴. Other acute myelopathies, such as autoimmune demyelinating disease and traumatic contusion injury, often involve some component of direct myelin and axonal injury in white matter with associated disruption of functionally significant ascending and descending white matter tracts²². The relative prognostic significance of GM pathology on MRI in this cohort of AFM patients reflects the primary injury mechanism of AFM and highlights the value of segmented evaluation of the spinal cord with distinct GM and WM maps. Interestingly, when the lesion involvement was measured relative to total cross-sectional area the correlation with motor outcomes was lost. Future studies with application of this technique to primary white matter diseases of the spinal cord would be of great interest for comparison.

The %GM T2 signal hyperintensity on a single axial slice at the most effected level of the injury center (referred to as "lesion center") provided the strongest correlation with clinical measures of motor impairment and recovery. The value of assessing transverse extent of T2 abnormality on a single axial slice at the injury center has been similarly demonstrated in the setting of acute traumatic spinal cord injury and compressive myelopathy^{18 25}, suggesting the transverse extent of injury in the spinal cord on MRI carries significant diagnostic

and prognostic information in a variety of pathologies. This result is significant as it allows for a more focused and rapid evaluation of the MRI findings centered at the injury center. The full lesion segment volume of %GM signal abnormality also significantly correlated with initial motor scores, and to a lesser extent with improvement. One potential advantage of full lesion segment volume calculation is that it does not rely upon the subjective determination of the most severely affected axial slice, thus potentially reducing variability and making analysis more conducive to a fully automated process. When the %GM involvement is calculated relative to the entire interrogated spinal cord gray matter volume, the significance of this measure with motor scores is lost, likely as a result of dilution of pathologic signal within significantly larger volumes of normal gray matter when lesions are not longitudinally extensive.

Potential applications for SCT in quantifying spinal cord pathology on MRI are vast and have the potential to greatly advance data-driven, unbiased approaches for assessing injury severity and guiding and monitoring therapy^{7, 9, 11, 20, 22, 26}. This proof-of-concept study validates the prognostic validity of this approach and demonstrates how segmented analysis of spinal cord subregions (i.e. %GM and %WM) may reflect the underlying pathophysiology of disease. Future studies incorporating analysis of specific white matter tract maps available in SCT and utilization of advanced quantitative MRI techniques, such as diffusion tensor imaging (DTI) and magnetization transfer imaging (MT), are needed²².

Limitations

The intramedullary T2 hyperintensity observed in our patients often resulted in obscuration of margins between SC and hyperintense CSF, thereby precluding automated spinal cord segmentation and necessitating manual approach for this step. An algorithm that can robustly and accurately segment the SC in patient populations with intramedullary T2 hyperintensity would reduce time and any bias associated with manual segmentation of the SC. In the current study, the segmentation and thresholding process were both reviewed by fellowship trained neuroradiologists; however, in order for large throughput analysis of patient SCs with minimal manual image post-processing, the propagated segmentation algorithm will need the capacity to propagate through axial slices with abnormal signal intensity. Another limitation in the current study is that signal abnormality below thoracic vertebral level 6 cannot be analyzed because the MNI-Poly-AMU template only covers C1 to T6 vertebral levels. This limitation resulted in one patient's most severe axial slice being excluded from analysis and the second-most being used. This limitation will be overcome with the future release of the new PAM50 template, which includes the brainstem and full spinal cord²⁷. Lastly, although fellowship trained neuroradiologists performed the manual thresholding steps for T2 image segmentation into a binary image defining the lesion area, this aspect of the study introduces potential bias. Future studies attempting to use SCT to quantify SC injury should adopt methods of automatic segmentation of lesions using Support Vector Machine (SVM) or

Random Forest algorithms. The study presented here is proof-of-concept to show the potential use of SCT to quantify abnormal signal in a population of patients with acute myelitis. Future studies will attempt a fully automated analysis pipeline, which further reduces user bias.

CONCLUSION

This proof-of-concept study utilized a recently developed open-source Spinal Cord Toolbox for atlas-based analysis of T2 signal abnormality in the spinal cord of 9 patients with AFM occurring during the EV-D68 outbreak in the western United States. This cluster of patients showed distinctive spinal cord lesions of the anterior central gray matter, characteristic of EV myelopathy, with variable WM involvement. An image processing and analysis pipeline was developed to register thresholded T2 MR images to the MNI-Poly-AMU template, enabling calculation of %WM, %GM, and %CSA pathology. Quantitative measures of %GM signal abnormality on a single axial slice at the most severely affected level of the injury epicenter were significantly associated with clinical outcome scores and MRC Strength Scores, reflecting the underlying pathophysiology for these patients with acute flaccid myelitis. Additionally, weighted averages of %GM involved in whole lesion segment were significantly correlated with MRC Strength Scores. %GM segmented calculations outperformed %WM and %CSA for predicting motor outcome. To date, this is the first study to use an atlas-based approach to quantify T2 measures of pathology in the spinal cord and correlate extracted metrics with clinical outcomes.

REFERENCES

1. Pons-Salort M, Parker EP, Grassly NC. The epidemiology of non-polio enteroviruses: recent advances and outstanding questions. *Current opinion in infectious diseases*. 2015 Oct;28(5):479-87. PubMed PMID: 26203854.
2. Greninger AL, Naccache SN, Messacar K, Clayton A, Yu G, Somasekar S, et al. A novel outbreak enterovirus D68 strain associated with acute flaccid myelitis cases in the USA (2012-14): a retrospective cohort study. *The Lancet Infectious diseases*. 2015 Jun;15(6):671-82. PubMed PMID: 25837569.
3. Messacar K, Schreiner TL, Maloney JA, Wallace A, Ludke J, Oberste MS, et al. A cluster of acute flaccid paralysis and cranial nerve dysfunction temporally associated with an outbreak of enterovirus D68 in children in Colorado, USA. *Lancet*. 2015 Apr 25;385(9978):1662-71. PubMed PMID: 25638662.
4. Diseases DoV. National Centers for Immunization and Respiratory Diseases, CDC. Notes from the field: acute flaccid myelitis among persons aged ≤ 21 years—United States. CDC. August 1-November 13, 2014;2015;63(53):1243-1244(MMWR Morb Mortal Wkly Rep).

5. Maloney JA, Mirsky DM, Messacar K, Dominguez SR, Schreiner T, Stence NV. MRI findings in children with acute flaccid paralysis and cranial nerve dysfunction occurring during the 2014 enterovirus D68 outbreak. *AJNR American journal of neuroradiology*. 2015 Feb;36(2):245-50. PubMed PMID: 25414005.
6. Baruah D, Chandra T, Bajaj M, Sonowal P, Klein A, Maheshwari M, et al. A simplified algorithm for diagnosis of spinal cord lesions. *Current problems in diagnostic radiology*. 2015 May-Jun;44(3):256-66. PubMed PMID: 25801464.
7. Fonov VS, Le Troter A, Taso M, De Leener B, Leveque G, Benhamou M, et al. Framework for integrated MRI average of the spinal cord white and gray matter: the MNI-Poly-AMU template. *NeuroImage*. 2014 Nov 15;102 Pt 2:817-27. PubMed PMID: 25204864.
8. Cohen-Adad J DLB, Benhamou M, Cadotte D, Fleet D, Cadotte A, Fehlings MG, Pelletier Paquette JP, Thong W, Taso M, Collins DL, Callot V, Fonov V. Spinal Cord Toolbox: an open-source framework for processing spinal cord MRI data. *Proceedings of the 20th Annual Meeting of OHBM, Hamburg, Germany 2014*;3633.
9. Levy S, Benhamou M, Naaman C, Rainville P, Callot V, Cohen-Adad J. White matter atlas of the human spinal cord with estimation of partial volume effect. *NeuroImage*. 2015 Oct 1;119:262-71. PubMed PMID: 26099457.
10. Ullmann E, Pelletier Paquette JF, Thong WE, Cohen-Adad J. Automatic labeling of vertebral levels using a robust template-based approach. *International journal of biomedical imaging*. 2014;2014:719520. PubMed PMID: 25132843. Pubmed Central PMCID: 4123554.
11. Yiannakas MC, Mustafa AM, De Leener B, Kearney H, Tur C, Altmann DR, et al. Fully automated segmentation of the cervical cord from T1-weighted MRI using PropSeg: Application to multiple sclerosis. *NeuroImage Clinical*. 2016;10:71-7. PubMed PMID: 26793433. Pubmed Central PMCID: 4678307.
12. Martin AR DLB, Aleksanderek I, Cohen-Adad J, Cadotte DW, Kalsi-Ryan S, Tetreault L, Crawley AP, Ginsberg H, Mikulis D, Fehlings MG. A Prospective Longitudinal Study in Degenerative Cervical Myelopathy Using Quantitative Microstructural MRI with Tract-Specific Metrics. *Proceedings of the 24th Annual Meeting of ISMRM, Singapore*. 2016.
13. Okuda DT, Mowry EM, Cree BA, Crabtree EC, Goodin DS, Waubant E, et al. Asymptomatic spinal cord lesions predict disease progression in radiologically isolated syndrome. *Neurology*. 2011 Feb 22;76(8):686-92. PubMed PMID: 21270417. Pubmed Central PMCID: 3053327.
14. Schlaeger R, Papinutto N, Zhu AH, Lobach IV, Bevan CJ, Bucci M, et al. Association Between Thoracic Spinal Cord Gray Matter Atrophy and Disability in Multiple Sclerosis. *JAMA neurology*. 2015 Aug;72(8):897-904. PubMed PMID: 26053119.
15. Kearney H, Miller DH, Ciccarelli O. Spinal cord MRI in multiple sclerosis--diagnostic, prognostic and clinical value. *Nature reviews Neurology*. 2015 Jun;11(6):327-38. PubMed PMID: 26009002.
16. Bede P, Bokde AL, Byrne S, Elamin M, Fagan AJ, Hardiman O. Spinal cord markers in ALS: diagnostic and biomarker considerations. *Amyotrophic lateral sclerosis : official publication of the World Federation of Neurology Research Group on Motor Neuron Diseases*. 2012 Sep;13(5):407-15. PubMed PMID: 22329869.

17. Mabray MC, Talbott JF, Whetstone WD, Dhall SS, Phillips DB, Pan JZ, et al. Multidimensional Analysis of Magnetic Resonance Imaging Predicts Early Impairment in Thoracic and Thoracolumbar Spinal Cord Injury. *Journal of neurotrauma*. 2016 Feb 1. PubMed PMID: 26414451.
18. Talbott JF, Whetstone WD, Readdy WJ, Ferguson AR, Bresnahan JC, Saigal R, et al. The Brain and Spinal Injury Center score: a novel, simple, and reproducible method for assessing the severity of acute cervical spinal cord injury with axial T2-weighted MRI findings. *Journal of neurosurgery Spine*. 2015 Oct;23(4):495-504. PubMed PMID: 26161519.
19. Jenkinson M, Beckmann CF, Behrens TE, Woolrich MW, Smith SM. Fsl. *NeuroImage*. 2012 Aug 15;62(2):782-90. PubMed PMID: 21979382.
20. De Leener B, Kadoury S, Cohen-Adad J. Robust, accurate and fast automatic segmentation of the spinal cord. *NeuroImage*. 2014 Sep;98:528-36. PubMed PMID: 24780696.
21. Tihan T. Pathologic approach to spinal cord infections. *Neuroimaging clinics of North America*. 2015 May;25(2):163-72. PubMed PMID: 25952171.
22. Martin AR, Aleksanderek I, Cohen-Adad J, Tarmohamed Z, Tetreault L, Smith N, et al. Translating state-of-the-art spinal cord MRI techniques to clinical use: A systematic review of clinical studies utilizing DTI, MT, MWF, MRS, and fMRI. *NeuroImage Clinical*. 2016;10:192-238. PubMed PMID: 26862478. Pubmed Central PMCID: 4708075.
23. Evans AC, Janke AL, Collins DL, Baillet S. Brain templates and atlases. *NeuroImage*. 2012 Aug 15;62(2):911-22. PubMed PMID: 22248580.
24. Jubelt B, Lipton HL. Enterovirus/picornavirus infections. *Handbook of clinical neurology*. 2014;123:379-416. PubMed PMID: 25015496.
25. You JY, Lee JW, Lee E, Lee GY, Yeom JS, Kang HS. MR Classification System Based on Axial Images for Cervical Compressive Myelopathy. *Radiology*. 2015 Aug;276(2):553-61. PubMed PMID: 25906184.
26. Hendrix P, Griessenauer CJ, Cohen-Adad J, Rajasekaran S, Cauley KA, Shoja MM, et al. Spinal diffusion tensor imaging: a comprehensive review with emphasis on spinal cord anatomy and clinical applications. *Clinical anatomy*. 2015 Jan;28(1):88-95. PubMed PMID: 24497009.
27. De Leener B TM, Fonov VS, Le Troter A, Stikov N, Collins DL, Callot V, Cohen-Adad J. Fully--integrated T1, T2, T2*, white and gray matter atlases of the spinal cord. . Proceedings of the 24th Annual Meeting of ISMRM, Singapore. 2016.

Case	Age	Sex	Limb Weakness	MRC Composite Score	Enterovirus Detected	MRC Score at Follow-up	Discharge Diagnosis
1	3	M	RUE	11	NP Swab	2	Disease due to EV
2	7	M	Bilateral LE	20	None	3	Encephalomyelitis, Paraesthesia/hyperesthesia
3	4	F	Bilateral LE	9	None	1	Flaccid paralysis, unspecified
4	8	M	RUE	9	NP Swab	0	Acute Flaccid Paralysis
5	27	M	Bilateral LE	1	Serum	3	Virus-related myelitis
6	38	F	LUE	16	None	2	Viral Meningitis
7	24	M	Bilateral LE	24	None	3	Meningomyelitis
8	10	M	LUE	18	None	2	Post Infectious Mycoplasma Transverse Myelitis
9	2	F	LUE	3	None	1	Hopkin's Syndrome

Table 1: Clinical description of 9 AFM patients used in analysis. Abbreviations: M, male; F, female; L, left; LE, lower extremities; M, male; NP, nasopharyngeal; R, right; UE, upper extremities.

152x47mm (150 x 150 DPI)

Peer Review




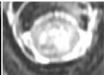
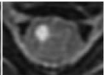
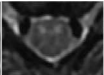
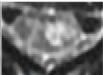
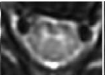





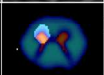




									
									
	Patient 1	Patient 2	Patient 3	Patient 4	Patient 5	Patient 6	Patient 7	Patient 8	Patient 9
	Vertebral Level T6	Vertebral Level C3	Vertebral Level C3	Vertebral Level C3	Vertebral Level C4	Vertebral Level C4	Vertebral Level C2	Vertebral Level C4	Vertebral Level T2
Lesion Center Percent (STD)	GM: 69.8 (46.0)	GM: 51.1 (45.9)	GM: 87.2 (33.4)	GM: 80.0 (40.0)	GM: 34.7 (47.6)	GM: 17.9 (38.4)	GM: 43.9 (49.6)	GM: 34.1 (47.4)	GM: 0.0 (0.0)
	WM: 45.1 (49.8)	WM: 26.7 (44.2)	WM: 20.9 (40.7)	WM: 28.1 (44.9)	WM: 4.4 (20.4)	WM: 5.4 (22.6)	WM: 11.8 (32.3)	WM: 1.2 (1.1)	WM: 41.8 (49.3)
Lesion Segment Percent (STD)	GM: 65.5 (47.5)	GM: 55.6 (49.7)	GM: 83.2 (37.4)	GM: 33.2 (47.1)	GM: 17.6 (38.1)	GM: 8.0 (27.2)	GM: 41.2 (49.2)	GM: 14.2 (34.9)	GM: 13.2 (33.9)
	WM: 27.0 (44.4)	WM: 26.1 (43.9)	WM: 20.8 (40.6)	WM: 9.3 (29.0)	WM: 3.5 (18.3)	WM: 5.3 (22.4)	WM: 11.7 (32.1)	WM: 0.30 (5.5)	WM: 57.3 (49.5)
Full Cord Atlas volume Percent (STD)	GM: 17.3 (37.8)	GM: 18.7 (39.0)	GM: 83.2 (37.4)	GM: 5.3 (22.4)	GM: 10.0 (30.00)	GM: 9.3 (29.1)	GM: 41.8 (49.3)	GM: 6.0 (23.7)	GM: 16.8 (37.4)
	WM: 4.4 (20.6)	WM: 20.6 (40.4)	WM: 20.8 (40.6)	WM: 1.7 (13.0)	WM: 2.0 (14.1)	WM: 7.3 (26.1)	WM: 11.9 (32.3)	WM: 0.8 (9.3)	WM: 53.4 (49.9)
CSA Lesion Center Percent (STD)	CSA: 47.3 (50.0)	CSA: 34.5 (47.5)	CSA: 26.7 (44.2)	CSA: 31.9 (46.6)	CSA: 6.9 (25.3)	CSA: 8.4 (27.7)	CSA: 14.6 (35.3)	CSA: 4.6 (20.9)	CSA: 38.9 (48.7)
CSA Lesion Segment Percent (STD)	CSA: 29.5 (45.6)	CSA: 30.7 (46.1)	CSA: 27.5 (44.7)	CSA: 11.5 (32.0)	CSA: 4.9 (21.6)	CSA: 6.9 (25.4)	CSA: 14.4 (35.1)	CSA: 1.8 (13.3)	CSA: 56.5 (49.6)

Table 2: First Row: Axial T2 image from center of lesion. Second Row: Probabilistic GM and WM map overlaid on thresholded axial T2 image from lesion center. Lesion Center: %WM and %GM weighted average metrics at axial lesion center. Lesion Segment: %WM and %GM weighted average metrics for lesion segment. Full Chord Atlas Volume: %WM and %GM weighted average metrics for full cord atlas volume. CSA Lesion Center: %CSA weighted average metrics at axial lesion center. CSA Lesion Segment: %CSA weighted average metrics at lesion segment

362x280mm (150 x 150 DPI)



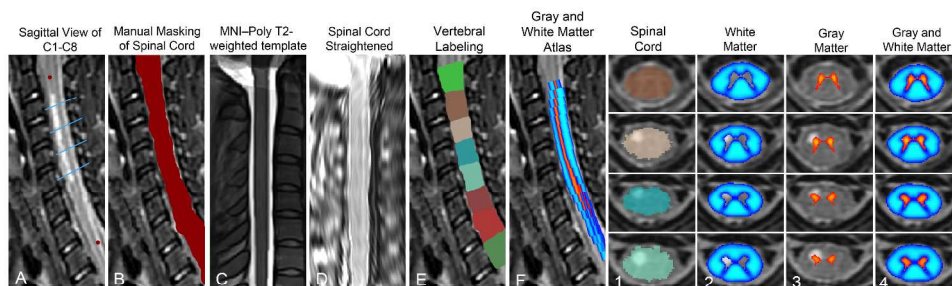


Figure 1: Steps for registering AFP Patient 1 to template. A: Red Circles indicate manual marking of anatomical features C1 and C8. Blue lines indicate axial slices illustrated in far right grid. B: Manual masking of spinal cord centerline was done at each axial slice due to signal hyperintensity interfering with automatic reconstruction of centerline. C: MNI-Poly T2-weighted template. D: Spinal cord straightening using thin-plate spline interpolation. E: Labeling of vertebral levels after registering to template and warping back to native space. F: Sagittal view of gray and white matter probabilistic atlas after registering to template and warping back to native space. Far Right Grid: Output of template-based atlas. Column 1: Automatic vertebral body labeling and spinal cord space. Column 2: Probabilistic masks of white matter. Column 3: Probabilistic masks of gray matter. Column 4 Probabilistic masks of gray and white matter overlaid.

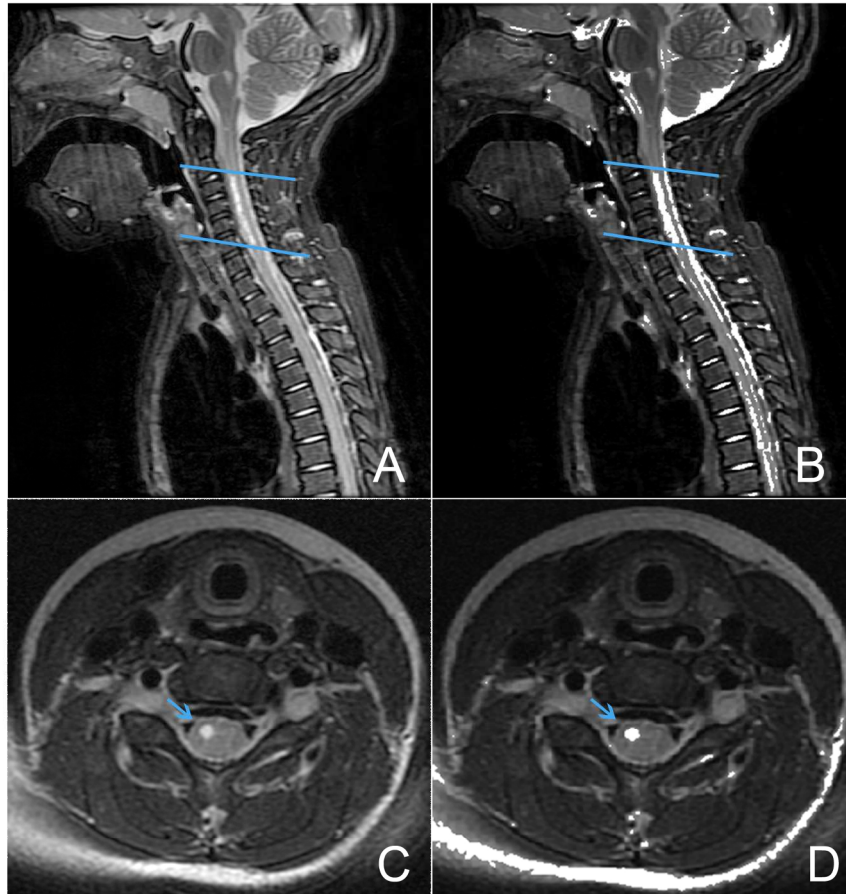


Figure 2: MRI images of patient No. 1. A: Sagittal plane T2 weighted image centered on lesion. B: Overlay of binary thresholded image for lesion and T2 weighted sagittal image. C: Axial T2 weighted image at lesion center. D: Overlay of binary thresholded image for lesion and T2 weighted axial image.

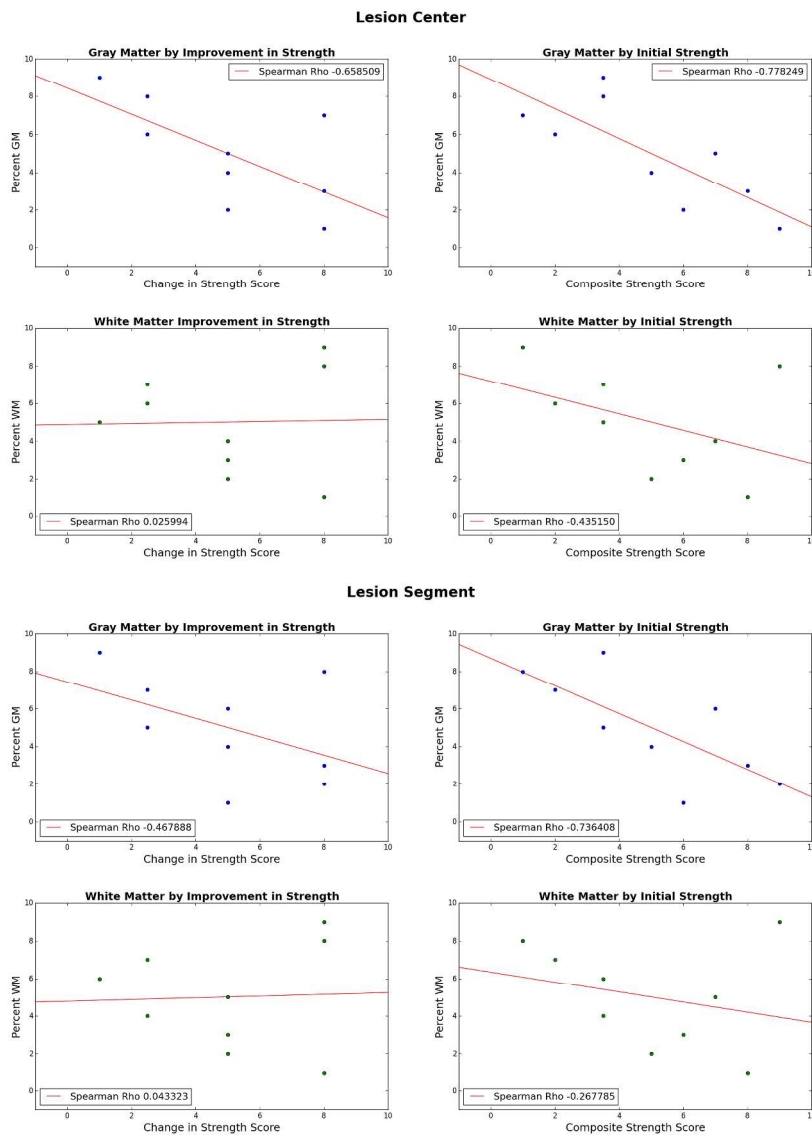


Figure 3. Scatter plots of numeric outcome clinical outcome score/MRC strength score by weighted average metric ranking for gray and white matter separated by analysis types (Lesion Center and Lesion Segment).

American Journal of Neuroradiology

Transfer of Copyright Agreement, Conflict of Interest Acknowledgment, Certification of
Coauthors, and Exclusive Publication Statement

Manuscript No. _____

Date: 4/25/2016

Complete copyright to the article entitled:

MRI atlas-based measurement of spinal cord injury predicts outcome in acute flaccid myelitis

is hereby transferred to the American Society of Neuroradiology (for United States government employees to the extent transferable), effective if and when the article is accepted for publication in the *American Journal of Neuroradiology*. In the case of the authors who are officers or employees of the United States government, the American Society of Neuroradiology recognizes that works prepared by officers or employees of the United States government as part of their official governmental duties are in the public domain.

Authors reserve all proprietary rights other than copyright, such as patent rights and the right to use all or part of this article in future works of their own. The authors retain the right of replication, subject only to crediting the original source of publication and receiving written permission from the publisher.

The authors certify that:

- 1) **This manuscript contains no matter that is libelous or otherwise unlawful, invades individual privacy, or infringes on any proprietary rights.**
- 2) **They have fulfilled the requirements of their employer's Institutional Review Board.**
- 3) **They will receive no royalty or other compensation from the American Society of Neuroradiology.**
- 4) **They will notify the editor of any proprietary or commercial interest or conflicts of interest the authors may have that relate directly or indirectly to the subject of this article.**
- 5) **They have made substantive and specific intellectual contributions to the article and assume public responsibility for its content.**
- 6) **They have reviewed and approved the final version of the manuscript.**
- 7) **None of the material in this manuscript has been published previously or is currently under consideration for publication elsewhere.**
- 8) **This copyright agreement has been signed by all authors.**

Name (print) <u>David McCoy</u>	Signature	
Name (print) <u>Jason Talbott</u>	Signature	
Name (print) <u>Michael Wilson</u>	Signature	
Name (print) <u>Mark Mamlouk</u>	Signature	
Name (print) <u>Julien Cohen-Adad</u>	Signature	
Name (print) <u>Mark Wilson</u>	Signature	
Name (print) <u>Jared Narvid</u>	Signature	
Name (print) _____	Signature	_____
Name (print) _____	Signature	_____

This signed statement must be received **before** the manuscript can be processed for publication. If there are problems obtaining any signatures, please contact the editorial office. You may return the signed form (photocopies/faxes are acceptable) to:

American Journal of Neuroradiology

800 Enterprise Drive, Suite 205

Oak Brook, IL 60523

630.574.1487 • FAX 630.788.6251

ScholarOne Support: (434) 964-4100